Scripta Materialia 146 (2018) 327–330

Contents lists available at ScienceDirect

Scripta Materialia

journal homepage: www.elsevier.com/locate/scriptamat

Regular article

# Room temperature plasticity in m-$Al_{13}Co_4$ studied by microcompression and high resolution scanning transmission electron microscopy

S. Korte-Kerzel [a,*], V. Schnabel [b,1], W.J. Clegg [b], M. Heggen [c]

[a] Institute of Physical Metallurgy and Metal Physics, RWTH Aachen University, Germany
[b] Department of Materials Science and Metallurgy, University of Cambridge, UK
[c] Ernst Ruska-Centre, Forschungszentrum Jülich GmbH, Germany

ARTICLE INFO

*Article history:*
Received 12 November 2017
Received in revised form 12 December 2017
Accepted 13 December 2017
Available online 4 January 2018

*Keywords:*
Plasticity
Complex metallic alloy
Dislocations
HR-TEM
Microcompression

ABSTRACT

In several complex crystals, like $Al_{13}Co_4$, metadislocations have been shown to facilitate plastic flow at high temperature. Consistent deformation has been revealed in small scale testing down to room temperature, but until now, no high resolution studies of the underlying dislocation core structures have been conducted to confirm the presence of metadislocations where diffusion slows down towards room temperature. Here, we used microcompression and high resolution TEM to reveal that room temperature plasticity in the monoclinic $Al_{13}Co_4$ phase does indeed occur by motion of metadislocations and that these are closely related to those reported previously in the orthorhombic $Al_{13}Co_4$ phase.



Complex crystals exhibit structural symmetries proscribed to simpler, conventional crystals. In particular in quasi-crystals and their approximants, their unique topology and electronic structure gives rise to interesting magnetic, optical and mechanical properties [1,2]. Despite their large unit cells, most complex crystals are known to exhibit dislocation or phase transformation mediated plastic deformation [3–8], but the details of the underlying mechanisms are often not yet fully understood. An open question in this context is whether previously identified deformation mechanisms at high temperatures involving the motion of a large number of atoms [9,10] or synchronous movement of atoms in different directions [3,11] may take place in a similar way at room temperature. Here, we elucidate this question using two complementary experimental techniques: (i) nanomechanical single crystal compression tests, which have been shown to successfully suppress cracking in many brittle crystals [6,7,12] including quasicrystals and Laves phases, and (ii) high resolution scanning transmission electron microscopy to study the dislocation core structure generated in deformation at room temperature and thus under conditions where a much more limited contribution of diffusion to the deformation process would be expected.

As an example of some of the most complex yet well-studied structures, we use $Al_{13}Co_4$, a quasicrystal approximant and complex metallic alloy [10,13–16]. In this and related structures, extended defects, called metadislocations, have been found in high temperature deformation experiments and their structure has been revealed in detail by electron microscopy [10,15]. Metadislocations are highly complex partial dislocations mediating plastic deformation as well as phase transformations in many complex metallic alloy phases [4]. They are observed in various alloy systems like Al–Pd–Mn [17–19] and $Al_{13}Co_4$ [10,15]. In the phase o-$Al_{13}Co_4$, for instance, the atomic structure of metadislocation cores with six and four stacking faults was revealed using high-resolution high angle annular dark field scanning transmission electron microscopy (HAADF-STEM). Burgers vectors of $-b/\tau^4$ [010] and $b/\tau^3$ [0 1 0], respectively, were found, where $\tau = \frac{\sqrt{5}+1}{2}$ is the number of the golden mean. The metadislocations are associated to separate phason defects, which are required to adapt the dislocation core structure to the o-$Al_{13}Co_4$ phase and which escort their movement through the material. Due to the complex nature of the defect itself and the large number of atoms inside the core region taking part in structural rearrangement upon movement, the atomic mechanism of metadislocation motion is elusive. By combining high-resolution HAADF-STEM, density functional theory, and simulated annealing, a first three-dimensional model of a metadislocation glide step in o-$Al_{13}Co_4$ was recently presented [16]. A single glide step implies the motion of about 250 atoms along various crystallographic with maximum atomic jump distances of 3.4 Å.

The defects investigated in all previous studies were, however, introduced in high temperature macroscopic compression tests. Therefore, the question remains if such highly complex deformation mechanisms

* Corresponding author.
*E-mail address:* korte-kerzel@imm.rwth-aachen.de (S. Korte-Kerzel).
[1] Now at: Laboratory for Nanometallurgy, ETH Zurich, Switzerland.

https://doi.org/10.1016/j.scriptamat.2017.12.015

involving extensive structural rearrangements of the material occur at room temperature as well. Recent results using small scale testing revealed that $Al_{13}Co_4$ [5,20] and quasicrystals [6] can be deformed plastically down to room-temperature if cracking is suppressed by reducing the specimen size [7,21]. This enables the dislocation structures induced in low temperature compression experiments to be studied in detail. Here, we present the first work revealing the dislocation core structure in an $Al_{13}Co_4$ crystal deformed at room temperature using high-resolution HAADF-STEM. As the approximate composition $Al_{13}Co_4$ exists in two crystal structures [22] which are very closely related (Fig. 1A), we focus here on the monoclinic phase, which has not been studied before. However, the results presented here are expected to not only extend previous studies to a related phase but to be complementary in the sense that the dislocation mechanisms are expected to be closely related, with the monoclinic phase formed during metadislocation movement in the orthorhombic phase [10], and that if similar metadislocation structures form and move in the absence of increased thermal activation at high temperature in the monoclinic phase, the same might reasonably be expected for the orthorhombic phase.

The monoclinic $Al_{13}Co_4$ phase is homeotypic to that of monoclinic $Al_{13}Fe_4$, and structurally closely related to o-$Al_{13}Co_4$ [13,14,23,24]. The two dimensional tiling description of the monoclinic phase (Fig. 1A) viewed along the b direction is characterized by a parallel arrangement of pentagon/rhomb elements whereas the orthorhombic phase is described by an alternating arrangement of pentagon/rhomb elements. In order to describe vectors within the tiling representation, we use a cubic basis spanned by the vectors a′ and c′ with the edge length of idealized tiles (approximately 4.7 Å). In terms of this basis the monoclinic cell is spanned by the vectors $\mathbf{a} = (\tau\sqrt{\tau+2}\ \ 1)$ and $\mathbf{c} = (0\ \ \tau+1)$. The orthorhombic cell is spanned by the vectors $(\tau\sqrt{\tau+2}\ \ 0)$ and $(0\ \ \tau+1)$, respectively.

A polycrystalline sample was arc-melted from the elements and characterized by X-ray diffraction (XRD) revealing that the major constituents were the orthorhombic and monoclinic $Al_{13}Co_4$ phases (Fig. 1A and B). After mechanical grinding and polishing, the sample was mapped by electron back-scatter diffraction (EBSD) to reveal the local orientation. Due to the high similarity of the two phases their distinction by EBSD is not reliable in all orientations and an orientation map including both phases is therefore shown in Fig. 1C. Grains of different resolved shear stresses on the two expected slip planes ((001) in o-$Al_{13}Co_4$ [5,15,20] and (100) in m-$Al_{13}Co_4$) could be identified due to the equivalent symmetry and micropillars were prepared by focussed ion beam (FIB) milling in several grains with a range of resolved shear stresses (Fig. 1D). The final beam current for thinning used was 100 pA at an accelerating voltage of 30 kV. After compression using a flat punch diamond indenter at room temperature, all pillars were imaged from four sides and a TEM lamella was extracted from the micropillar shown in Fig. 1E after compression. Conventional TEM confirmed the m-$Al_{13}Co_4$ crystal structure of the single crystal micropillar and the operation of the expected (100) plane revealed by diffraction (Fig. 1F). The same lamella was then thinned further to allow high resolution HAADF-STEM analysis.

The stress-strain curves obtained on all pillars were analysed in terms of the first visible deviation from linear elastic loading, taken as the yield stress, and the measured values are shown in Fig. 2a. The three sets of compression experiments performed at rates of 0.02, 0.2 and 2 mN $s^{-1}$ show an overall constant stress level at the onset of yielding within the scatter that is common to most microcompression studies [25]. A distinction may be made between those pillars which

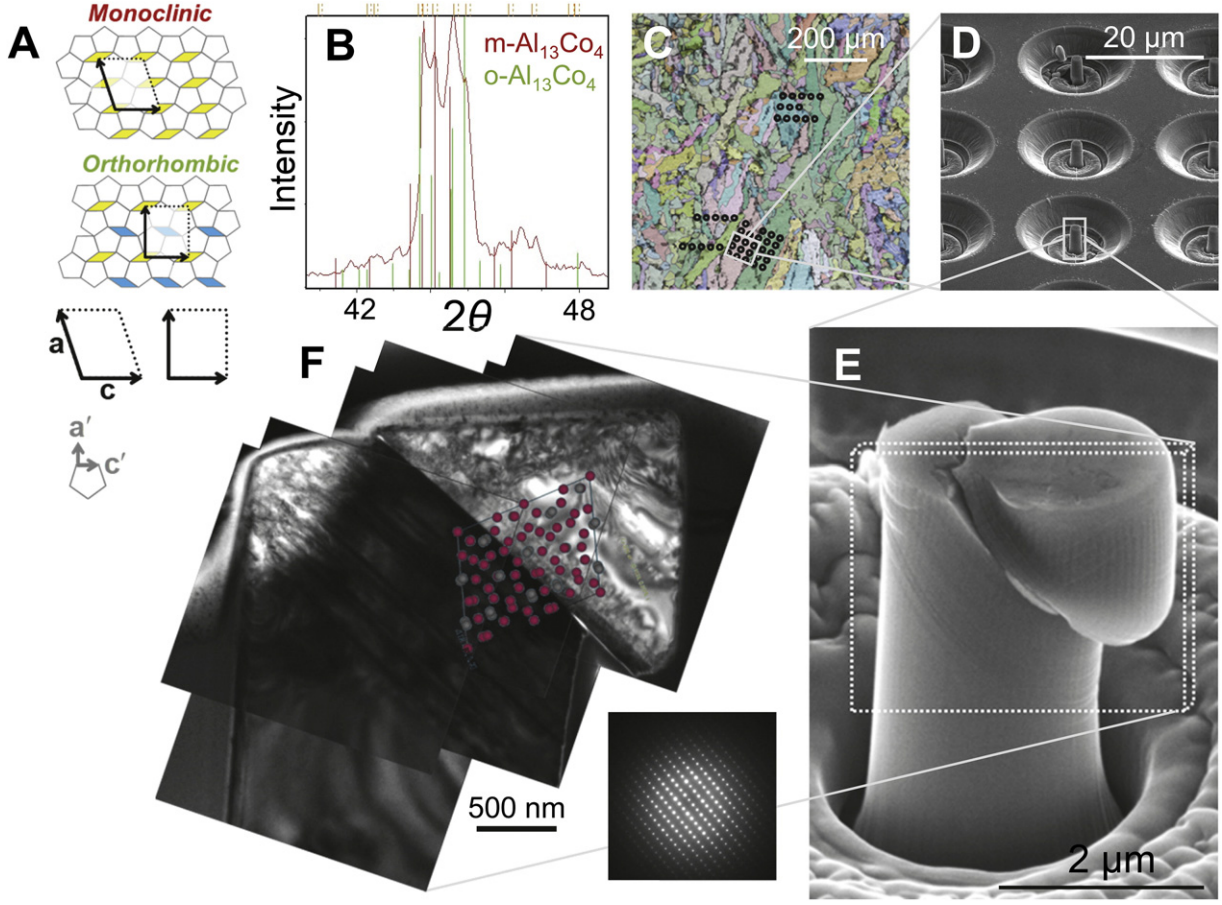


**Fig. 1.** (A) Tiling representation of m- and o-$Al_{13}Co_4$ with base vectors and unit cells indicated for both structures. The presence of both m- and o-$Al_{13}Co_4$ was confirmed by XRD (B) and the orientation was determined locally by EBSD (C). Micropillars were prepared by FIB (D) at the positions indicated by circles in (C). A compressed micropillar (E, secondary electron micrograph) was further analysed in a centre cross-section by conventional TEM (F, bright field image and selected area diffraction pattern).

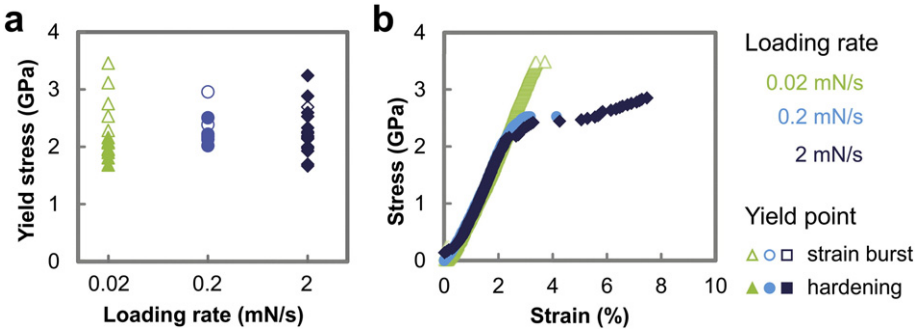


**Fig. 2.** (a) Yield stresses of pillars tested at three different loading rates. Those pillars which exhibited stable yielding are represented by closed symbols while those where yielding was associated with a displacement burst are given as open symbols. Typical stress-strain curves are given in (b) with the micropillar analysed by (HR)TEM shown in dark blue.

showed stable deformation after yielding and those which exhibited a displacement burst as the first visible sign of plastic deformation (see Fig. 2b). These two sets are shown as filled and open symbols in Fig. 2, respectively, and reveal that a small rate dependence may be present for plasticity by defect glide, while in the case of displacement bursts no rate dependence is seen. However, no clear distinction can be made based on the stress-strain curves and the corresponding SEM images between burst events mediated by nucleation of dislocations or cracks or a sequence of both as found in previous work on brittle crystals [7,21,26]. The yield stresses are consistent with the stresses reported on the orthorhombic phase using a single crystal specimen at room temperature [20], suggesting that both phases deform at a similar stress level at room temperature. Taking those pillars most similar to the curves measured by Walter et al. [20] with small load drops in displacement control, i.e. those showing no or small strain bursts here, a comparable rate sensitivity at room temperature was found. The implication of this finding is that the activation volumes for glide are of the same order in the m- and o-$Al_{13}Co_4$ phases and that therefore the underlying deformation mechanisms not only extend from high to room temperature in the orthorhombic phase, as suggested in [20], but are also very similar in both crystal structures.

In order to reveal the type of dislocation facilitating plastic flow in the m-$Al_{13}Co_4$ phase at room temperature, conventional TEM and HAADF-STEM was employed on a micropillar which had exhibited a large amount of stable plastic deformation. Its appearance with parallel slip traces formed in the top half of the pillar, shown in the scanning electron micrograph in Fig. 1E, is consistent with plastically deformed pillars of o-$Al_{13}Co_4$ where the Schmid factor on the (001)[010] slip system was high [20]. In pillars of varying other orientations slip and brittle as well as ductile fracture was observed but no clear distinction between the behaviour of the two $Al_{13}Co_4$ phases can be made based on the EBSD analysis due to the similarity of the structures. However, there was also no obvious difference in the behaviour of those pillars indexed with a high confidence as either the orthorhombic or monoclinic phase.

Fig. 3a shows a Bragg-contrast bright-field TEM image of dislocations (white arrows) and stacking faults (black and grey arrows) of the plastically deformed pillar. The structure of the stacking faults is revealed by using high-resolution HAADF-STEM in Fig. 3b. Using a pentagon/rhomb tiling description, the stacking fault extending along the c-direction is represented by three rows of pentagon/rhomb elements (blue tiles in Fig. 3), which are twinned with respect to the matrix. Stacking faults extending along the (1 0 −2) direction (grey arrow) are represented using additional phason elements (red tiles in Fig. 3). The formation of twin-like stacking faults and single phason defects was observed in plastically deformed o-$Al_{13}Co_4$ as well, however, the formation of straight stacking faults involving phason elements was not observed.

Fig. 4 present microstructural investigations using HAADF-STEM of two different dislocation cores and their associated stacking faults using the pentagon/rhomb tiling. Again, the stacking fault of the dislocation in Fig. 4 a is represented by three rows of pentagon/rhomb elements (blue tiles in Fig. 4b). The core of the dislocation is identified by a green polygon and a Burgers circuit is performed using unstrained tiles. The Burgers vector of the dislocation is $b'_1 = (0 \quad \frac{1}{\tau^2})$, i.e. $\frac{1}{\tau^4}c$ or approximately 1.80 Å along the c direction (Fig. 4c).

The second dislocation presented in Fig. 4d has a distinctly larger core area and is connected to five twin-like rows of pentagon/rhomb tiles (blue tiles in Fig. 4e). The tiling representation furthermore demonstrates the existence of a phason defect (red tile in Fig. 4e) which alters the stacking sequence of the pentagon/rhomb elements at the right-hand side of the dislocation core (compare Ref [10]). A representation of the dislocation core structure without the phason element would be possible as well (compare Fig. 3d in Ref [10]). The Burgers vector of the dislocation in Fig. 4f $b'_2 = -(0 \quad \frac{1}{\tau^3})$ is smaller than $b_1$ by a factor of $\tau$, i.e. $\frac{1}{\tau^5}c$ or approximately 1.11 Å along the −c direction.

The dislocation core structures and Burgers vectors observed in m-$Al_{13}Co_4$ in the present work are equal to those observed in o-$Al_{13}Co_4$

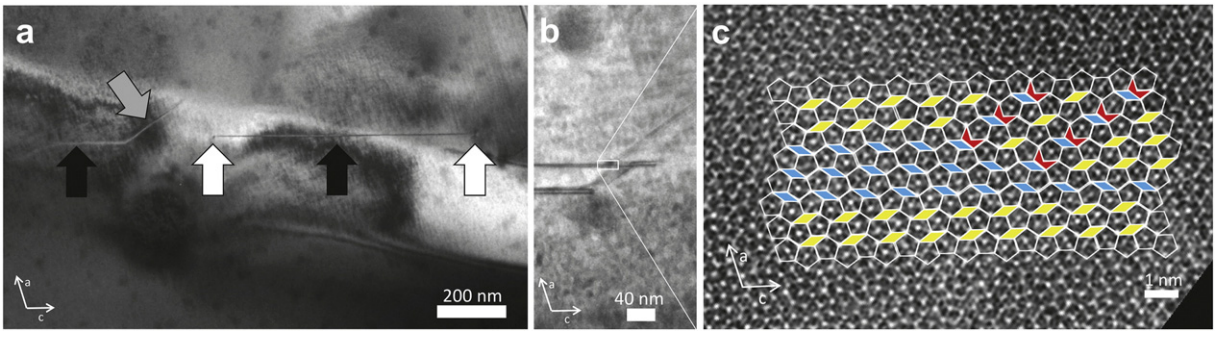


**Fig. 3.** (a) Bragg-contrast bright-field TEM image of dislocations (white arrows) and stacking faults (black and grey arrows). (b) Additional TEM image and (c) high-resolution HAADF-STEM image of the boxed region in (b) with tiling representation of stacking faults.

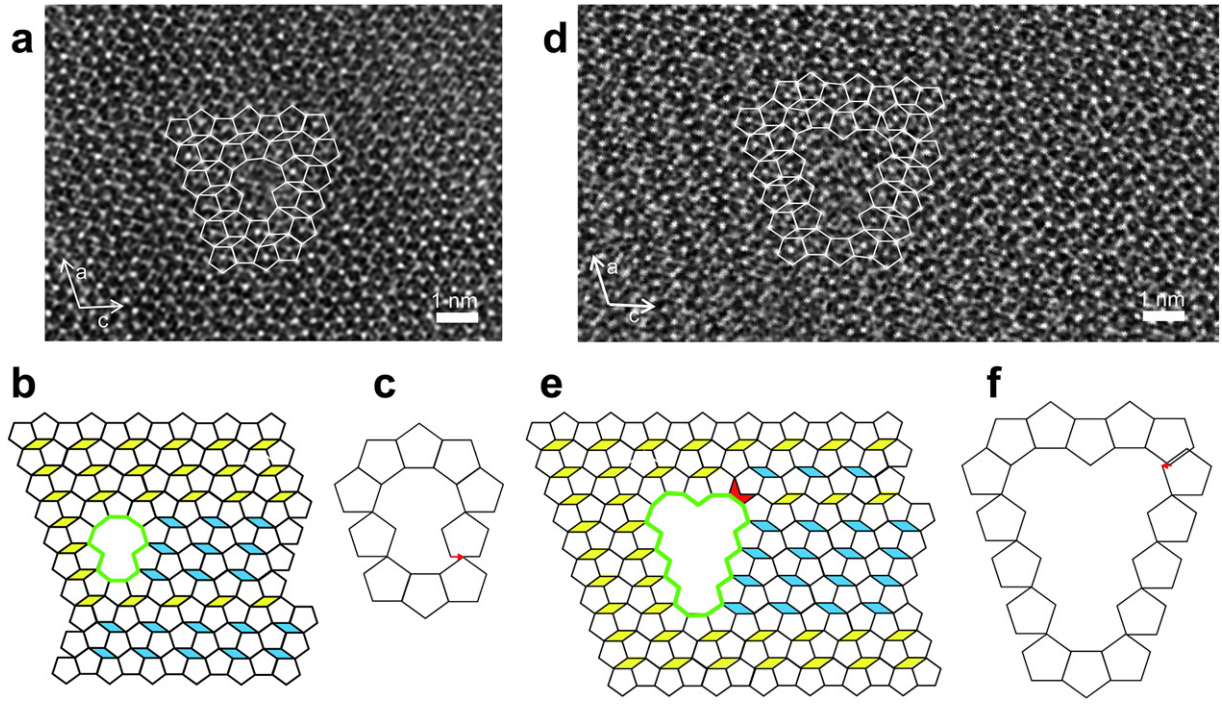


**Fig. 4.** (a, d) HAADF-STEM images of two different metadislocation cores, (b, e) tiling representation, and (c, f) a Burgers circuit using unstrained tiles.

after deformation at high temperature [10]. Assuming that the Burgers vector has no component along the b direction, which is true for dislocations in o-$Al_{13}Co_4$ as well, the dislocation would be of pure edge-type and would move by glide. The only difference between dislocations in o- and m-$Al_{13}Co_4$ however is the necessity to introduce additional phason defects into the o-$Al_{13}Co_4$ structure in order to accommodate the dislocation core structure (compare Figs. 2 & 3 in Ref. [10]). The addition of phason elements is possible in m-$Al_{13}Co_4$ (Fig. 4f) as well, but is not required to accommodate the dislocation (compare Figs. 5 and 3b–d in Ref [10]).

Using microcompression to suppress fracture and conventional and high resolution TEM to elucidate the operative slip planes and dislocation core structures, we show that room temperature deformation in the monoclinic $Al_{13}Co_4$ phase occurs by motion of metadislocations even at room temperature. No discernible differences in terms of the critical stresses for deformation on the crystallographically equivalent planes, rate sensitivity or deformation morphology were found for the two crystal structures of monoclinic and orthorhombic $Al_{13}Co_4$. High-resolution HAADF-STEM of a deformed micropillar demonstrates the presence of a complex deformation mechanism based on the motion of metadislocations at room temperature in monoclinic $Al_{13}Co_4$. From a comparison with an idealized tiling, we infer that two types of metadislocations with $b_1 = (0 \quad 0 \quad \frac{1}{\tau^2})$ and $b_2 = -(0 \quad 0 \quad \frac{1}{\tau^3})$ associated to three and five stacking faults represented by twin-like rows of pentagon/rhomb elements exist.

The structure of the metadislocations observed in the present work is widely comparable to those observed in o-$Al_{13}Co_4$ after high-temperature plastic deformation, consistent with the similarities observed also in terms of the mechanical response of micropillars at room temperature. The structural similarities between the metadislocations observed in the present work and those in o-$Al_{13}Co_4$ implies the presence of a highly complex process of metadislocation motion similar to the atomic model of metadislocation glide in o-$Al_{13}Co_4$ recently presented [16]. The existence of a room-temperature deformation mechanism inducing structural transformations and atomic motion of hundreds of atoms along various crystallographic directions is perhaps surprising but an essential consequence of our present results.

## Acknowledgements

The work was supported by the EPSRC/Rolls-Royce Strategic Partnership (EP/M005607/1).

## References

[1] K. Deguchi, S. Matsukawa, N.K. Sato, T. Hattori, K. Ishida, H. Takakura, T. Ishimasa, Nat. Mater. 11 (12) (2012) 1013–1016.
[2] J. Dolinšek, Chem. Soc. Rev. 41 (20) (2012) 6730–6744.
[3] P. Hazzledine, P. Pirouz, Scr. Metall. Mater. 28 (10) (1993) 1277–1282.
[4] M. Feuerbacher, M. Heggen, in: J.P. Hirth, L. Kubin (Eds.), Dislocations in Solids, Elsevier, Amsterdam 2010, pp. 109–170.
[5] A. Bhowmik, I.P. Dolbnya, T.B. Britton, N.G. Jones, G. Sernicola, C. Walter, P. Gille, D. Dye, W.J. Clegg, F. Giuliani, Appl. Phys. Lett. 108 (11) (2016) 111902.
[6] Y. Zou, J.M. Wheeler, A.S. Sologubenko, J. Michler, W. Steurer, R. Spolenak, Philos. Mag. 96 (32–34) (2016) 3356–3378.
[7] S. Korte-Kerzel, MRS Commun. (2017) 1–12.
[8] J.T. Sypek, C.R. Weinberger, S. Vijayan, M. Aindow, S.L. Bud'ko, P.C. Canfield, S.-W. Lee, Scr. Mater. 141 (2017) 10–14.
[9] M. Feuerbacher, S. Balanetskyy, M. Heggen, Acta Mater. 56 (8) (2008) 1849–1856.
[10] M. Heggen, M. Feuerbacher, Mater. Res. Lett. 2 (3) (2014) 146–151.
[11] M.F. Chisholm, S. Kumar, P. Hazzledine, Science 307 (5710) (2005) 701–703.
[12] S. Korte, W.J. Clegg, Adv. Eng. Mater. 14 (11) (2012) 991–997.
[13] R. Hudd, W. Taylor, Acta Crystallogr. 15 (5) (1962) 441–442.
[14] K. Saito, K. Sugiyama, K. Hiraga, Mater. Sci. Eng. A 294 (2000) 279–282.
[15] M. Heggen, L. Houben, M. Feuerbacher, Philos. Mag. 88 (13–15) (2008) 2333–2338.
[16] M. Heidelmann, M. Heggen, C. Dwyer, M. Feuerbacher, Scr. Mater. 98 (2015) 24–27.
[17] H. Klein, M. Feuerbacher, P. Schall, K. Urban, Phys. Rev. Lett. 82 (17) (1999) 3468–3471.
[18] M. Heggen, L. Houben, M. Feuerbacher, Nat. Mater. 9 (4) (2010) 332.
[19] M. Heggen, L. Houben, M. Feuerbacher, Acta Mater. 59 (11) (2011) 4458–4466.
[20] C. Walter, J. Wheeler, J. Barnard, R. Raghavan, S. Korte-Kerzel, P. Gille, J. Michler, W. Clegg, Acta Mater. 61 (19) (2013) 7189–7196.
[21] F. Östlund, P.R. Howie, R. Ghisleni, S. Korte, K. Leifer, W.J. Clegg, J. Michler, Philos. Mag. 91 (7–9) (2011) 1190–1199.
[22] T. Gödecke, M. Ellner, Z. Met. 87 (11) (1996) 854–864.
[23] J. Grin, U. Burkhardt, M. Ellner, K. Peters, J. Alloys Compd. 206 (2) (1994) 243–247.
[24] J. Grin, U. Burkhardt, M. Ellner, K. Peters, Z. Krist. 209 (6) (1994) 479–487.
[25] M.D. Uchic, P.A. Shade, D.M. Dimiduk, Annu. Rev. Mater. 39 (2009) 361–386.
[26] F. Östlund, K. Rzepiejewska-Malyska, K. Leifer, L.M. Hale, Y. Tang, R. Ballarini, W.W. Gerberich, J. Michler, Adv. Funct. Mater. 19 (15) (2009) 2439–2444.